In Situ Observation of the On-Surface Thermal Dehydrogenation of n-Octane on Pt(111)

Daniel Arribas[a], Víctor Villalobos-Vilda[a], Ezequiel Tosi[a,b], Paolo Lacovig[b], Alessandro Baraldi[b,c], Luca Bignardi[c], Silvano Lizzit[b], José Ignacio Martínez[a], Pedro Luis de Andres[a,d], Alejandro Gutiérrez[e,f], José Ángel Martín-Gago[a], and Pablo Merino[a]

[a] *Instituto de Ciencia de Materiales de Madrid, c/ Sor Juana Inés de la Cruz, 3 (Spain)*
[b] *Elettra-Sincrotrone, S.C.p.A., S.S. 14km 163.5, Trieste (Italy)*
[c] *Department of Physics, University of Trieste, Via Valerio 2, 34127 Trieste (Italy)*
[d] *On leave of absence at nanoteeche@surfaces Laboratory, Swiss Federal Laboratories for Materials Science and Technology, 8600-Dübendorf (Switzerland)*
[e] *Applied Physics Department, Universidad Autónoma de Madrid, Calle Francisco Tomás y Valiente, 7, 28049 Madrid (Spain)*
[f] *Instituto Nicolás Cabrera, Calle Francisco Tomás y Valiente, 7, 28049 Madrid (Spain)*

Table of contents

1- Thermal programmed desorption rate model

We introduce a model based on population dynamics equations to fit the TPD spectrum displayed in **Fig. 1a** [1–4]. As explained in the main text, our experimental results reveal that *n*-octane undergoes the following dehydrogenation scheme: First, above 330 K, physisorbed *n*-octane (C_8H_{18}) suffers a single dehydrogenation at one of its methyl ends and chemisorbs (C_8H_{17}). Second, above 600 K, chemisorbed molecules undergo a fast dehydrogenation at two adjacent carbon atoms yielding a double bond within the carbon skeleton (C_8H_{15}). To fit our TPD data we propose that these reactions behave as first order processes governed by rate constants, K_1 and K_1, that follow the Arrehnius law $K_i = A_i \cdot exp\left(\frac{-E_i}{kT}\right)$. Here, A_i corresponds to the pre-exponential factor, E_i to the activation energy for the i-*th* reaction, which are used as

fitting parameters. Molecular rehydrogenation, has a negligible impact at temperatures above the recombinative desorption onset, after which the population of on-surface hydrogen atoms is almost zero due to rapid recombination. For simplicity, it has not been considered in our final model. High-temperature shoulders appearing near each TPD peak (see **Fig. 1a**) are attributed to coverage-dependent or substrate-adsorbate interactions arising at defective regions of the surface, which increment dehydrogenation energy barriers. The rate constants K_1^{def} and K_2^{def} govern the dehydrogenation reactions of the molecules adsorbed in these regions. The set of equations 1-6 describes the population dynamics of the *n*-octane adsorbates and a scheme of the reaction is presented in **Fig. S1**.

$$(1)\quad \frac{d[C_8H_{18}]}{dt} = -K_1 \cdot [C_8H_{18}]$$

$$(2)\quad \frac{d[C_8H_{18}{}^{def}]}{dt} = -K_1{}^{def} \cdot [C_8H_{18}{}^{def}]$$

$$(3)\quad \frac{d[C_8H_{17}]}{dt} = \left(K_1 \cdot [C_8H_{18}] + K_1{}^{def} \cdot [C_8H_{18}{}^{def}]\right) \cdot \alpha_1 - K_2 \cdot [C_8H_{17}]$$

$$(4)\quad \frac{d[C_8H_{17}{}^{def}]}{dt} = \left(K_1 \cdot [C_8H_{18}] + K_1{}^{def} \cdot [C_8H_{18}{}^{def}]\right) \cdot (1-\alpha_1) - K_2{}^{def} \cdot [C_8H_{17}{}^{def}]$$

$$(5)\quad \frac{d[C_8H_{15}]}{dt} = \left(K_2 \cdot [C_8H_{17}] + K_2{}^{def} \cdot [C_8H_{17}{}^{def}]\right) \cdot \alpha_2$$

$$(6)\quad \frac{d[R_{no\,H}]}{dt} = \left(K_2 \cdot [C_8H_{17}] + K_2{}^{def} \cdot [C_8H_{17}{}^{def}]\right) \cdot (1-\alpha_2)$$

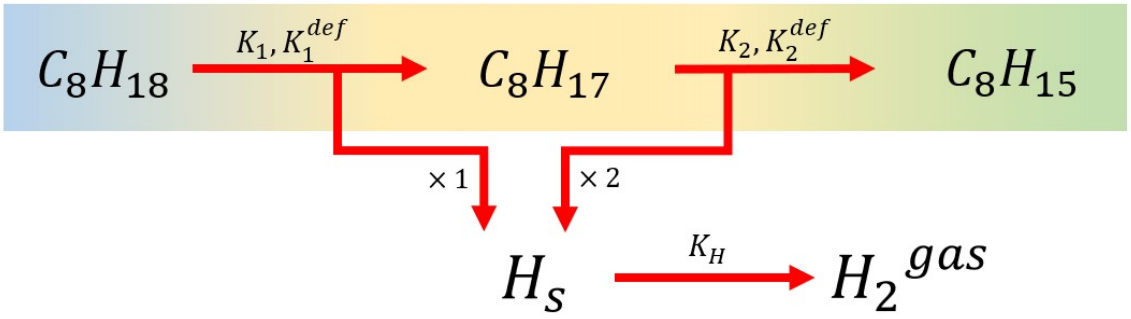

Figure S1. Scheme of the dehydrogenation reactions releasing atomic hydrogen adsorbed on the surface and recombinative desorption of the latter as molecular hydrogen.

The ratio between the initial populations of $[C_8H_{18}]$ and $[C_8H_{18}{}^{def}]$ accounts for the intensity ratio of the hydrogen desorption peak, at 330 K, and its shoulder at 380 K. As the relative intensity peak/shoulder in the second dehydrogenation feature is different from that of the first feature (see **Fig. 1a**), the ratio between the produced $[C_8H_{17}]$ and $[C_8H_{17}{}^{def}]$ populations should

be different too. This means that populations at terraces and defective regions cannot be treated separately, but interconversion between adsorption configurations (e.g., due to diffusion) must be considered. The parameter α_1, a number in the interval $[0,1]$, effectively represents the fraction of chemisorbed molecules not suffering an increase of the second dehydrogenation energy barrier upon reaction (in the absence of further dehydrogenation, $\alpha_1 = [C_8H_{17}]/([C_8H_{17}{}^{def}] + [C_8H_{17}])$). This parameter accounts for the intensity ratio of the second dehydrogenation peak, at 600 K and its shoulder.

On the other hand, the integrated intensity of the second dehydrogenation feature (peak and shoulder) is lower than that of the first dehydrogenation. That suggests that either not all the chemisorbed alkane undergoes the second dehydrogenation described in our text or not all the hydrogen produced is desorbed and/or detected. The parameter α_2 corresponds to the fraction of molecules that suffer the second dehydrogenation producing detectable hydrogen and accounts for the reduced desorption of hydrogen at around 600 K. We denote as $[R_{no\,H}]$ the population of adsorbates coming from chemisorbed molecules not producing detectable hydrogen at 600 K. Processes such as molecular reforming, clustering or direct desorption of the adsorbates[5] or subsurface migration of the hydrogen at defective regions [6] can conciliate the chemical and morphological changes experimentally observed at this temperature with the observed reduced hydrogen desorption.

On-surface atomic hydrogen, $[H_s]$, and desorbed molecular hydrogen, $[H_2{}^{gas}]$, populations are treated independently in our model. Diffusion of on-surface atomic hydrogen on Pt(111) presents an energy barrier as low as 0.074 eV [3], so atomic hydrogen diffusion is considered to be much faster than its recombination and it is excluded from our model. Hydrogen recombination is considered to occur via a second-order reaction followed by immediate desorption at the experimental temperatures [1,6]. Dissociative readsorption of molecular hydrogen is neglected as desorbed hydrogen is assumed to be continuously pumped away. Equations 7 and 8 govern the populations of hydrogen.

$$\frac{d[H_s]}{dt} = K_1 \cdot [C_8H_{18}] + K_1{}^{def} \cdot [C_8H_{18}{}^{def}] + 2 \cdot \left(K_2 \cdot [C_8H_{17}] + K_2{}^{def} \cdot [C_8H_{17}{}^{def}]\right) \cdot \alpha_2 - 2K_H \cdot [H_s]^2 \quad (7)$$

$$\frac{d[H_2{}^{gas}]}{dt} = K_H \cdot [H_s]^2 \quad (8)$$

Our model does not explain the plateau feature appearing at 200 K, which is assumed to be related to desorption of unreacted *n*-octane molecules and the exposure to the vacuum of a higher area of the bare platinum surface.

For TPD fitting, pre-exponential factors (A_i), activation energies (E_i), and α_1 and α_2 were used as free parameters. The simulated TPD spectrum is calculated as the derivative of the

total desorbed hydrogen with respect to time, supposing a heating rate of 2 K/s. The fitting was obtained in two steps. First, we adjusted the pre-exponential factors and the energy barriers to obtain the position of the maxima of each peak and shoulder in agreement with the experimental spectrum. Pre-exponential factors were constrained to the interval from $5{\cdot}10^{12}$ s^{-1} to $5{\cdot}10^{13}$ s^{-1}. In the case of hydrogen desorption parameters, a good agreement with literature was also obtained [1,3,7]. Second, the initial populations $[C_8H_{18}]$ and $[C_8H_{18}{}^{def}]$ and parameters α_1 and α_2 parameters were adjusted so the relative intensities and general shapes of the peaks and shoulders match the observations. The experimental broadening of the spectrum is simulated by convoluting the resulting spectrum with a Gaussian function and the intensity has been normalized to the maximum of the experimental spectrum. The final TPD spectrum results are shown in **Table 1**.

TPD feature	A_i **(s^{-1})**	E_i **(eV)**	**Reaction**	**Calculated energy (eV)**
First peak	$1{\cdot}10^{13}$	0.85	$[C_8H_{18}]$ dehydrogenation	0.90
First shoulder	$1{\cdot}10^{13}$	1.06	$[C_8H_{18}{}^{def}]$ dehydrogenation	-
Second peak	$4{\cdot}10^{13}$	1.74	$[C_8H_{17}]$ dehydrogenation	2.01
Second shoulder	$4{\cdot}10^{13}$	2.02	$[C_8H_{17}{}^{def}]$ dehydrogenation	-
Hydrogen recombination	$1{\cdot}10^{13}$	0.87	Hydrogen recombination	0.92 ± 0.18[1,3,8,9]

Table S1. Parameters used to fit the TPD spectrum in **Figure 1** to our model (left part) and DFT calculated values for some reactions. Hydrogen recombination corresponds to the desorption of two hydrogen atoms as a molecule.

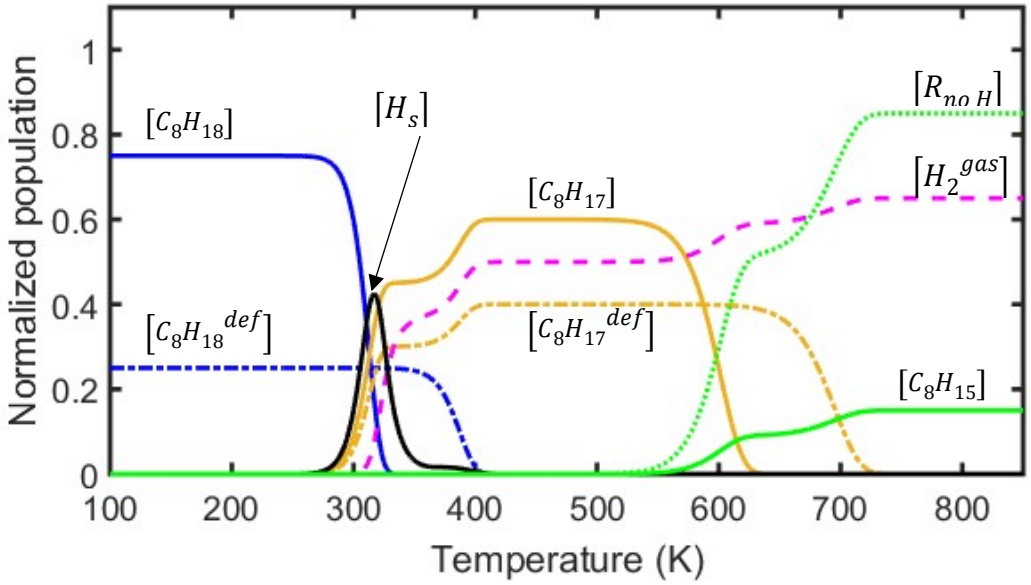

Figure S2. Evolution of the different populations as a function of time. The number of species has been normalized to the saturation coverage of physisorbed molecules if the Pt(111) surface was perfect. In this fit, $\alpha_1 = 0.6$ and $\alpha_2 = 0.15$.

Population evolution as a function of time is shown in **Fig. S2** for the spectrum fitted in **Fig. 1a** in the main text. According to our model, the onset of the first dehydrogenation occurs at around room temperature, but effective recombination of the released hydrogen atoms, $[H_s]$, takes place above 310 K, resulting in a temporary accumulation of chemisorbed hydrogen. The onset of the first dehydrogenation at defective regions takes place above 350 K. The second dehydrogenation reaction initiates at 550 K on the terraces and at 650 K on defective regions. At these temperatures, the desorption of hydrogen is too fast to allow atomic hydrogen to accumulate on the surface. The dashed magenta curve represents the total amount of molecular hydrogen desorbed from the surface and detected at the spectrometer.

2- Thermal evolution of the C1s XPS peak

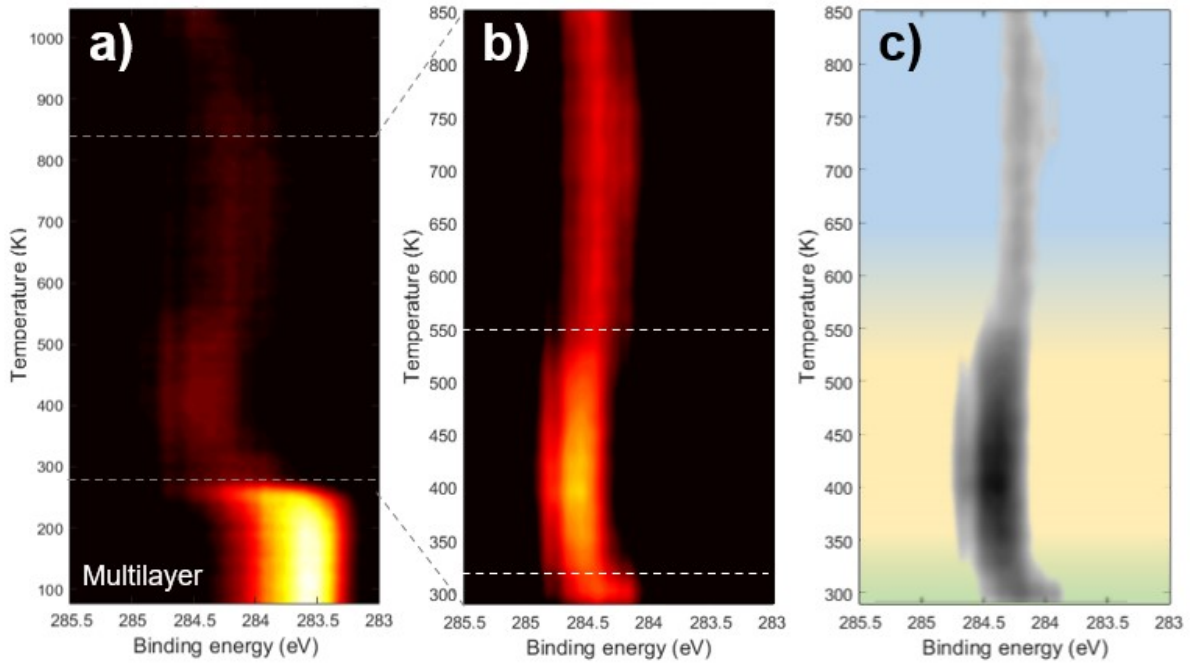

Figure S3. a) Thermal-programmed XPS map of the C 1s contribution of a saturated sample of *n*-C_8H_{18} dosed on Pt(111). The substrate was heated at rate of 2 K/s and each spectrum was acquired with an energy pass of 30 eV. b) Thermal-programmed XPS map acquired between 290 and 850 K, as indicated by the grey dashed lines in a) White lines separate the three dehydrogenation stages described in the main text. c) Same thermal-programmed XPS as in b) with background colors indicating the three dehydrogenation stages identified in our study (green: physisorption, yellow: chemisorption, blue: multiple dehydrogenation and cluster formation).

In this section we provide additional figures of the XPS characterization of *n*-octane. **Fig. S3a** and **b** shows the Temperature Programmed XPS (TP-XPS)[10] characterization of *n*-octane deposition on Pt(111). In the experiments, the surface was exposed to adsorbates until the total intensity of the C 1s spectra acquired during deposition reached a steady maximum, indicating saturation is reached. We annealed the sample following a temperature ramp of 2 K/s from 77 K to 1000 K and took XPS spectra in snapshot mode with an energy resolution of 10 meV. The energy range of the detector was set so that it covered the whole range of the spectrum to collect all the electrons simultaneously (snapshot mode) and reduce acquisition time to 3.2 seconds per spectrum.

At low temperatures, the high intensity of the multilayer forces us to use low photon fluxes to protect the detector, which rends signal at higher energies too dim at the temperatures of interest for our study. For that reason, a second TP-XPS experiment was conducted between 290 K and 850 K with a photon flux twice as high as in the previous case. Three chemically different regions can be clearly identified, separated with white dashed lines in **Fig S3b**. These lines coincide with the onset of the main hydrogen desorption peaks in **Fig. 1a**. No significant chemical changes occur at the temperatures at which shoulders appear in TPD spectra (390

K and 700 K), supporting the hypothesis that they are due to dehydrogenation of a small part of the adsorbates at higher temperatures in defective regions of the sample. Above 875 K progressive graphitization of the surface leads to formation of graphene patches, giving rise to a new peak at 284.5 eV [11] that corresponds to graphene. Above 1000 K, this peak becomes dominant over all the other contributions, indicating that adsorbates have completely dehydrogenated at these temperatures.

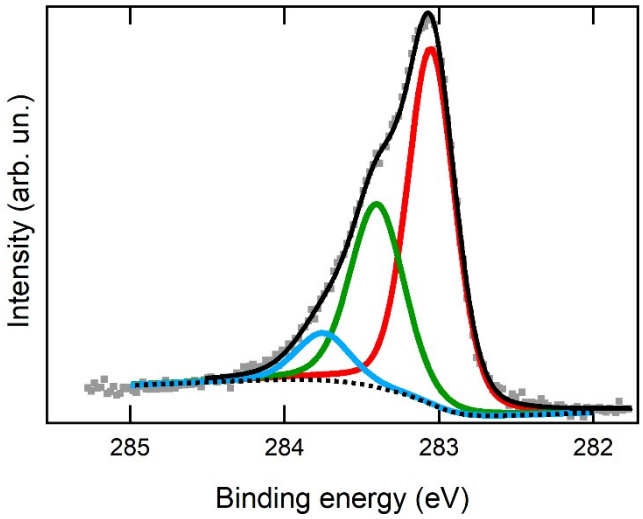

Figure S4. C-1s high-resolution XPS spectrum of a multilayer of *n*-octane after deposition on Pt(111) at 77 K without annealing. Three different peaks appear at 283.0, 283.4 and 283.8 eV. Relative intensities with respect to the peak at 283.0 eV are 1, 0.59 and 0.15 respectively.

A high-resolution spectrum of an as-prepared multilayer sample is shown in **Fig. S4**, in which three contributions at 283.0, 283.4, and 283.8 eV appear. As molecules of the multilayer interact with the surface in a different way than monolayer molecules do, direct correlation of these peaks with those of the physisorbed phase spectrum in **Fig. 1b** is not possible. We assign the most intense peak at 283.0 eV to the adiabatic photoionization of the carbon atoms of the *n*-octane and the other two to vibrational replicas of the main peak. Desorption of the multilayer phase occurs at a temperature of 290 K, with a 75% reduction of the total C 1s intensity (**Fig S4**).

Fig. S5 shows the intensity evolution of the main contributions analyzed in the main text (283.1, 283.5, 283.7, 283.9, and 284.4 eV) plus the graphene peak appearing at higher temperatures (284.5 eV, orange). This graph is the result of an automatized fitting of all the individual spectra of the TP-XPS map in **Fig S3**. We remark that the low signal-noise ratio of TP-XPS individual spectra only permit a qualitative interpretation of the spectra. A progressive reduction of the total intensity of the C 1s spectra with increasing temperature is observed, suggesting that desorption of some part of the adsorbates takes place.

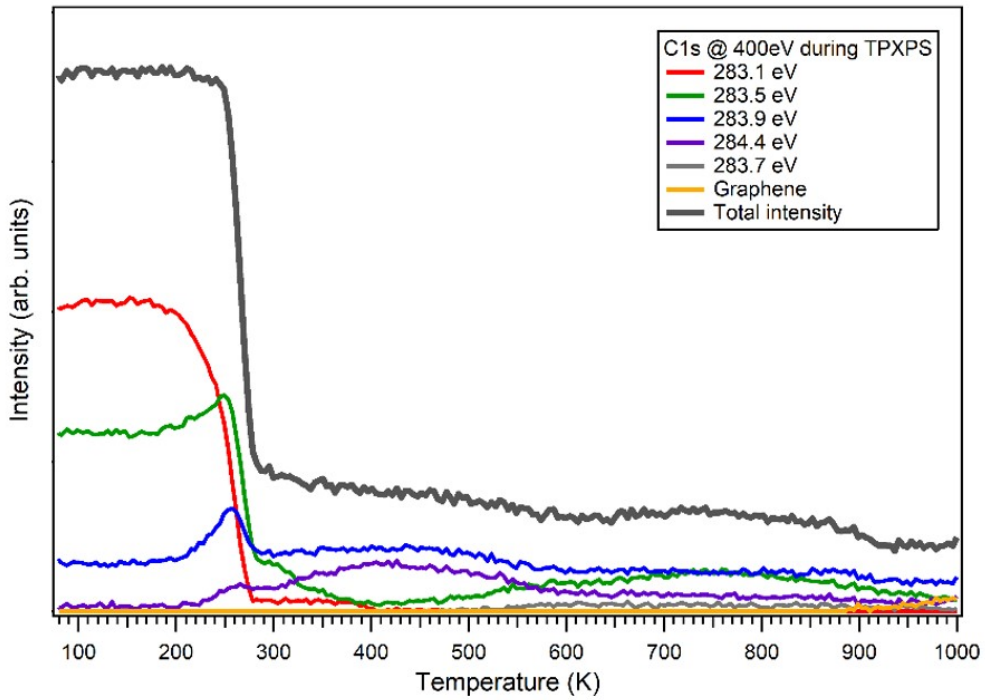

Figure S5. Relative intensities of the XPS contributions described in the main text (Fig 1b, c and d). The drop in intensity at 280 K corresponds to the desorption of the multilayer. Above 800 K a new contribution arises, assigned to graphene patches formed after deep dehydrogenation and aggregation of the adsorbates.

A quantitative analysis of the XPS intensities in the high-resolution spectra is shown in **Fig. S6**. Assignment of each contribution to a particular type of carbon atom constitutes a challenging task due to the complex vibrational profile that hydrocarbon contributions display (see main text). A precise quantitative analysis would require an exact knowledge of the energies and excitation probabilities of the C–H stretching modes at all the different dehydrogenation stages dehydrogenation, which cannot be easily obtained. For that reason, values shown in **Fig. S6b** are only approximated. To calculate them, we have subtracted first the intensity associated to the remnants of the multilayer, using the intensity of the peak at 283.0 eV and the ratio obtained from **Fig. S4**. This way, only the contributions from the monolayer were considered. Afterwards, assignment of intensities to each type of carbon atom was conducted considering the vibrational replicas due to simultaneous excitation of the C–H stretching modes.

The peak at 283.5 eV is related to $-CH_3$ groups. Its vibrational replica should appear at around 283.9 eV, which means that it coincides with the peak at 283.95 eV. Therefore, the accurate shape of the vibrational profile cannot be resolved. As a first approximation, to calculate the intensity of the replica we have assumed that the quotient of the intensities of the main peak and its vibrational replica are equal for the $-CH_3$ and $-CH_2-$ contributions (**Fig. S6b**). In the case of the peak at 283.7 eV (C–Pt), no vibrational replica is detected at around

284.1 eV, where it should be resolved from other peaks. This suggests that interaction with the surface hinders the excitation of the stretching modes at the surface-bound carbon atom.

At the second stage of dehydrogenation (600 K – 900 K) double bonds appear within the carbon skeleton of *n*-octane. As the photoelectrons from the corresponding carbon atoms present a binding energy around 283.4 eV, they cannot be distinguished from those coming from methyl-end carbon atoms. To estimate the intensity corresponding to each type of carbon atom, first we have assumed that the proportion of $-CH_3$ carbon atoms with respect to the total should remain approximately equal to that of the previous stage (this would be the case if dehydrogenation at this stage took place only at $-CH_2-$ carbon atoms as our DFT calculations suggest). After obtaining the intensity of the main $-CH_3$ and its replica, we assign the rest of the intensity to the $-CH=CH-$ carbon atoms.

a)

BINDING ENERGY (eV)	INTENSITY 290 K (arb. un.)	INTENSITY 373 K (arb. un.)	INTENSITY 675 K (arb. un.)
283.0 - 283.1	0.6	<0.1	-
283.4 - 283.5	2	1	1.6
283.7	-	0.95	1.2
283.95	3.2	3.1	1.6
284.4	1.2	1	0.6

b)

Type of carbon atom	INTENSITY 290 K (arb. un.)		INTENSITY 373 K (arb. un.)		INTENSITY 675 K (arb. un.)	
Multilayer	1.1	-	<0.1	-	-	-
$-CH_3$	2.0 ± 0.4	33% ± 7%	1.2 ± 0.2	20% ± 3%	0.9 ± 0.1	18% ± 2%
C–Pt	-	-	0.95	16%	1.2	24%
$-CH_2-$	4.0 ± 0.4	67% ± 7%	3.9 ± 0.2	64% ± 3%	2.0 ± 0.1	39% ± 2%
–CH=CH–	-	-	-	-	0.9 ± 0.1	18% ± 2%

Figure S6. a) Binding energies and intensities of the different contributions to the high-resolution C-1s XPS spectra in Fig. 1b, c and d. b) XPS intensities associated at the different chemically inequivalent carbon atoms of the adsorbates. after subtracting the intensity corresponding to the multilayer.

At the physisorbed state, *n*-octane presents two types of inequivalent carbon atoms: two $-CH_3$ and six $-CH_2-$. Our quantitative analysis approximately agrees with this proportion 1:3, but the intensity associated with $-CH_2-$ is slightly lower than expected. This fact suggests that C–H stretching excitation at the methyl end upon photoionization is less probable than at inner carbon atoms or that some modifications of the saturated carbon skeleton (e.g., fragmentation or isomerization) could be happening at defects. At the chemisorbed state, the adsorbates present three types of inequivalent carbon atoms: one $-CH_3$, six $-CH_2-$ and one C–Pt. Again, the proportion obtained from our estimations approximately agrees with this proportion, but

the $-CH_2-$ fraction is slightly lower than expected. At the second dehydrogenation stage, if all molecules underwent the double dehydrogenation explained in the main text (**Fig. 4**), adsorbates would present 4 types of inequivalent carbon atoms: one $-CH_3$, four $-CH_2-$, two $-CH=$ and one $C-Pt$. Our quantitative analysis suggests that there is a higher proportion of $C-Pt$ carbon atoms than expected and a lower proportion of double bonds and $-CH_2-$. This points to higher interaction of the adsorbates with the Pt surface and modifications within the carbon skeleton of the molecules.

3- Hydrocarbon fragments detected in TPD experiments

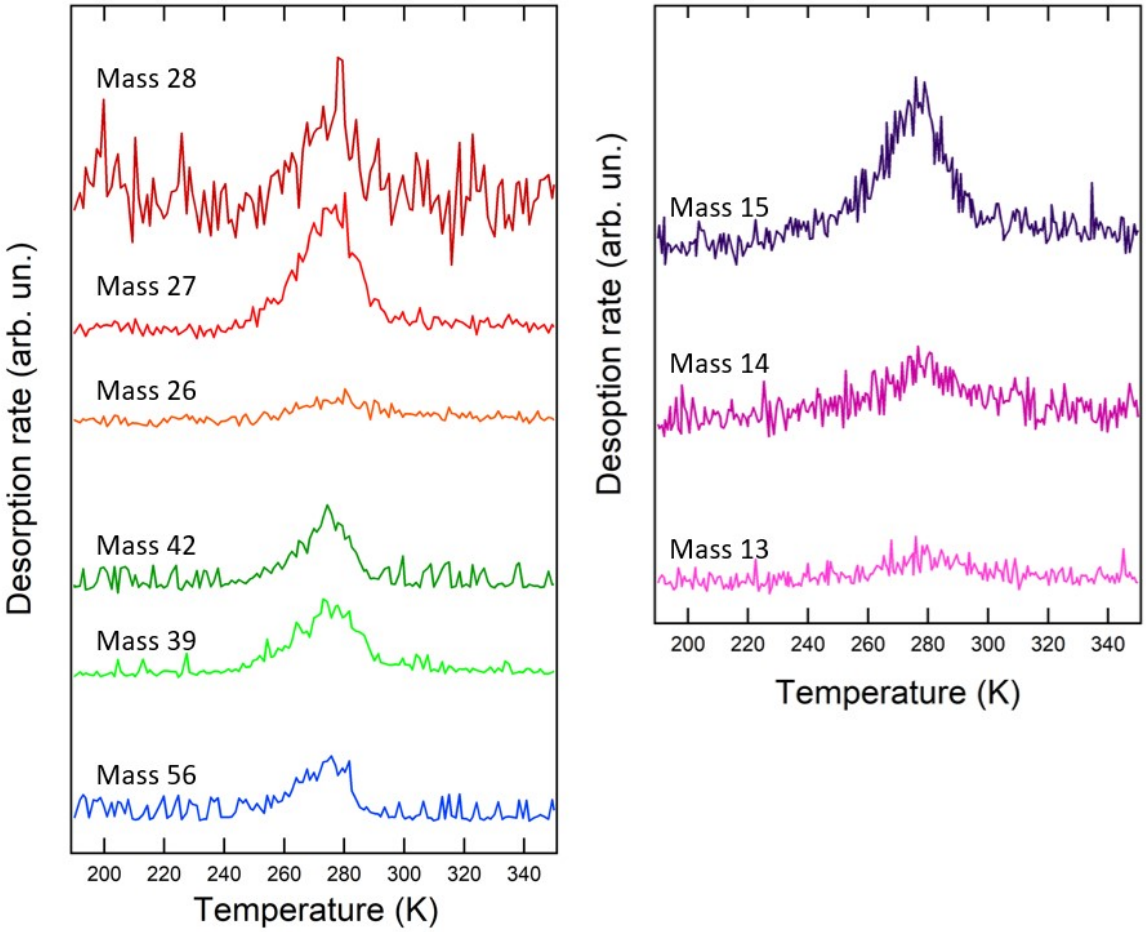

Figure S7. a), b) TPD spectra of C_xH_y fragments from corresponding to two different experiments. These fragments are produced by cracking of intact *n*-octane from the desorption of a dense monolayer phase. The maxima are located at around 275 K.

Fig. S7 displays the TPD spectra of the C_xH_y masses typically related to alkane fragmentation upon ionization at the mass spectrometer. Only between 250 and 290 K are these fragments detected. This range of temperatures coincides with the desorption of intact *n*-octane molecules from the multilayer from the Pt(111) surface as shown in TP-XPS maps (**Fig S3a**). In m/z= 2 spectra, this desorption coincides with the plateau feature that precedes the first dehydrogenation peak. At higher temperatures, these C_xH_y fragments were not detected, indicating that desorption of alkane, fragmented or not, is below the sensitivity of our mass spectrometer in the monolayer regime. This fact stems from the strong interaction between the adsorbates and the surface after formation of covalent C−Pt bonds.

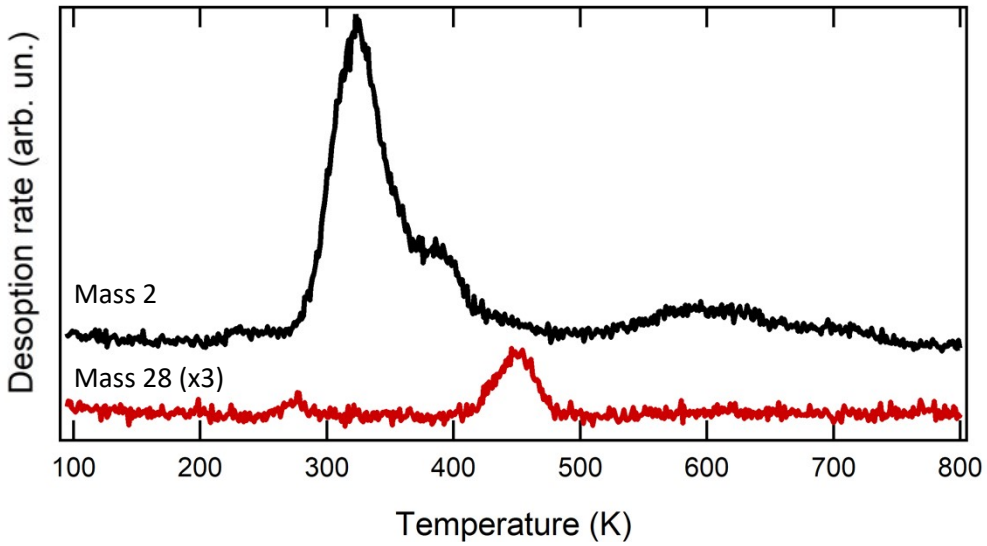

Figure S8. Mass/charge (m/z) 28 TPD spectrum, presenting two features with the maxima at 275 and 450 K. These features correspond to fragmentation of *n*-octane molecules desorbing from the multilayer and the desorption of CO molecules adsorbed from residual gas in the chamber. Mass 2 spectrum is also shown as reference.

Figure S8 shows the mass spectrum of mass 28 in the full range of temperatures of study (100-800 K). This spectrum displays two peaks, whose maxima are located at 275 K and 450 K respectively. The first one corresponds to fragmentation of intact molecules desorbed from the multilayer, as indicated in the previous paragraph. The peak at 450 K coincides with the desorption of CO molecules adsorbed from the residual gas at lower temperatures [12]. The previous does not interfere with our interpretation of the XPS C 1s spectra as the binding energy at which the CO peak appears (around 286.7 eV according to our experiments) is well above the range of energies analyzed in our work (281.75 – 285.5 eV).

4- Morphological characterization of the adsorbates in STM images

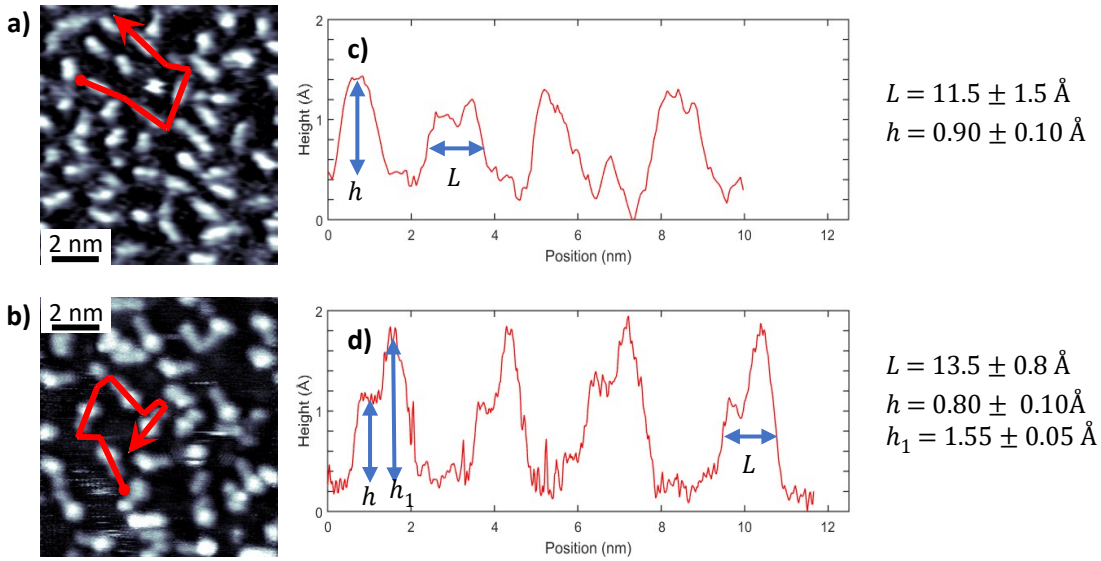

Figure S9. a), b): 10 nm x 10 nm STM images from main text corresponding to the physisorption, chemisorption and clustering stages. Red lines indicate the path along which profiles in panels d), e), and f) are acquired. d), e), f): Height profiles from the STM images in panels a), b), and c). The lengths (L) and heights (h, h_1) of the different features are calculated as the average of a large number of measurements and the errors as the standard deviation. Blue arrows indicate how these dimensions are measured.

Fig. S9 illustrates the procedure of morphological characterization of the adsorbate at each dehydrogenation stage. We took height profiles following multiple paths (e.g., those marked by the red arrows) to obtain a distribution of heights and lengths of an elevated number of adsorbates. Heights, h and h_1, were measured from the background at both sides of the feature to the average of the maximum-heights points as indicated in **Fig. S9c** and **d**. Lengths, L, correspond to the lateral distances between the half-maximum points at each side of the molecules. In the case of chemisorbed molecules, the half-maximum point at the lobed end corresponds to half the height of the protrusion, h_1. Values indicated in the figures has been obtained from the mean of a large number of measurements and the error margins are the standard deviations.

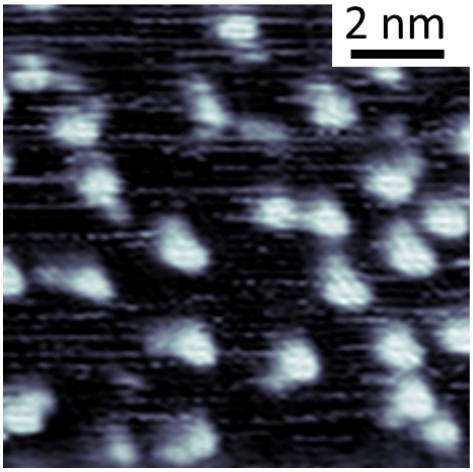

Figure S10. STM image acquired after *n*-octane deposition on Pt(111) at 520 K (V_{bias}= 1V, I = 0.165 nA). Features display the same morphology as those of in Fig. 3 (deposition at 400 K), proving that molecules remain chemisorbed at 520 K. Molecules still form a disordered phase, without significant aggregation, suggesting that diffusion is not effective at this temperature or that high lateral repulsion between adsorbates is still present.

We conducted additional STM measurements on *n*-octane sample after annealing at 520 K (**Fig. S10**), temperature right below the onset of the second dehydrogenation peak and above the first dehydrogenation shoulder in TPD mass-2 spectra (**Fig. 1a**). Adsorbates on the terraces conserve the same morphology described for samples annealed at 400 K (single-lobed rod-like features, see **Fig. 3** in the main text). This demonstrates that reactions giving rise to the first dehydrogenation shoulder are related to dehydrogenation at defective regions rather than to dehydrogenation at terraces, as indicated in the main text and **Section 1** of this supporting information. Molecules are still distributed in a disordered phase, indicating that diffusion, and subsequent aggregation, activates above 520 K.

5- Simulated highest occupied molecular orbitals

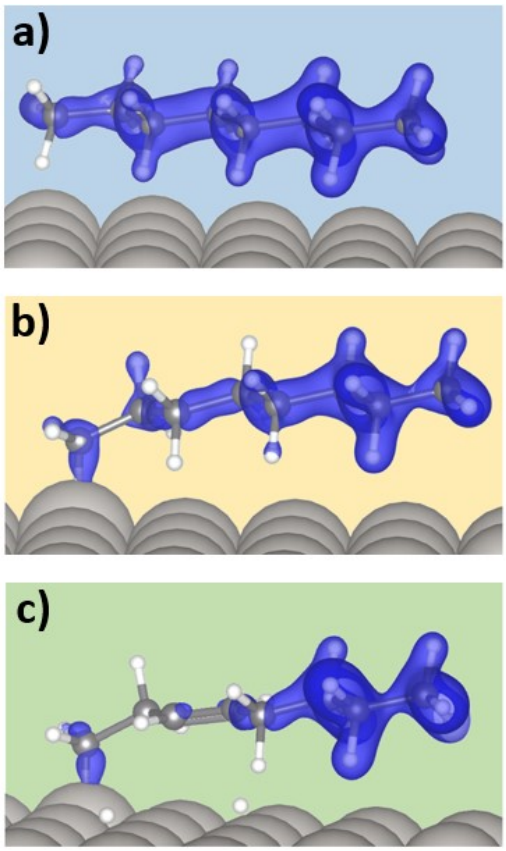

Figure S11. Isosurfaces containing 95% of the charge corresponding to the highest occupied molecular orbital states projected into the *n*-octane molecule for **a)** the physisorbed molecule, **b)** the chemisorbed molecule after first dehydrogenation, and **c)** molecule after a simultaneous double dehydrogenation yielding a double bond.

In **Fig. S11**, we show the projection on the molecules of the 95% charge density isosurfaces of the highest occupied molecular orbitals (HOMO) of the *n*-octane molecules physisorbed, chemisorbed, and chemisorbed after double bond formation between the third and fourth carbon atoms. The states related to the HOMO calculated to be located at bias voltages below -2.7 V. Interaction with the Pt(111) surface induces an asymmetry in the HOMO, even in the physisorbed state, that pushes the electrons away from the methyl end that points towards the surface. The diminished density of bonding states around this methyl end favors the cleavage of a C−H bond at the first carbon atom, while the charge density at the intact methyl end remains almost unaffected, making C−H bond cleavage there more unlikely. Once the C−Pt bond forms, a further decrease of the HOMO density is found around the hydrogen atoms at the third and fourth carbon atoms, favoring their subsequent dehydrogenation yielding a double bond. The charge density at the intact methyl end remains almost unaffected, making C−H bond cleavage there more unlikely.

In general, the C−H stretching vibrational modes are responsible for the approach of the H atom towards the catalytic surface. For that reason, C−H bond breaking will be favorable only at the hydrogen atoms that already protrude towards the surface at the lowest energy configuration of the adsorbate. Cleavage of other bonds not pointing towards the surface would require a considerable energy cost due to deformation of the molecule. Therefore, in this case, further dehydrogenation at the methyl end is highly unlikely compared to dehydrogenation at internal carbon atoms because, even though a significant decrease of the HOMO density happens at the remaining C−H bonds, they point away from the surface. In addition, further dehydrogenation at the methyl end would result in double or triple bond formation between the first carbon atom and the surface, which would force the molecule to adopt an energetically costly vertical configuration.

6- Calculation of the energy reaction path

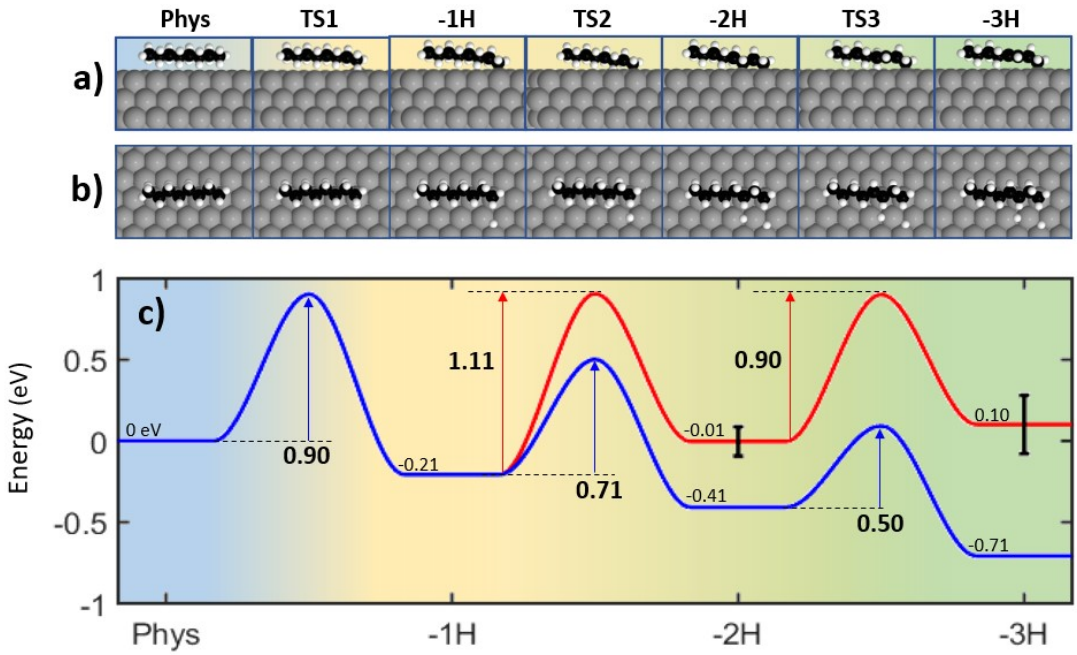

Figure S12. a), b): Lateral and top views of the different dehydrogenation stages of *n*-octane on Pt(111). c) Energy profile for the sequential dehydrogenation reactions of *n*-octane. The blue curve corresponds to the reaction energies maintaining all the products adsorbed on the surface, as obtained by DFT calculations. The adsorption energy of hydrogen produced in previous stages (E_H = –0.46 ± 0.09 eV per H atom) has been subtracted to obtain the red curve.

Figure S12c displays, for comparison, the as-calculated energy path for the dehydrogenation reactions (blue curve) and the effective energy path (red curve, see **Fig. 5c** in the main text) after subtracting the adsorption energy of the atomic hydrogen produced before the corresponding step. Accurate calculation of the energy path requires to keep the number of atoms constant during all the dehydrogenation steps. For that reason, in our calculations, we have constrained the hydrogen atoms separated from the molecule to remain adsorbed to the platinum surface (**Fig. S12a** and **S12b**). The as-calculated energy path follows the equation $\Delta E_0 = E_C - E_{ref}$, where E_C corresponds to the total calculated energy for each configuration along the reaction path and E_{ref} is the energy of the physisorbed state. However, TPD experiments show that hydrogen atoms undergo rapid recombination and desorption at the temperatures required for C−H bond cleavage. Therefore, the binding energy of the previously cleaved hydrogen atoms ($E_H = -0.46 \pm 0.09$ eV [1,3,8,9], see main text) in our simulations must be subtracted for a proper comparison with the experimental situation, yielding the effective energy path $\Delta E = E_C - E_{ref} - n \cdot E_H$[13,14] described in the main text.

If hydrogen desorption were not considered, all the sequential dehydrogenation reactions would be exothermic, presenting a decreasing energy barrier after each step. In that case,

once the first and higher energy barrier (0.90 eV) were overcome, the following sequential reactions would occur immediately. Since this contradicts our STM and XPS results, which indicate that most molecules remain singly dehydrogenated in the temperature range 350-550 K, we conclude that hydrogen removal is required for an accurate description of the dehydrogenation process.

8- Supplementary references

[1] B. Poelsema, K. Lenz, G. Comsa, *J. Chem. Phys.* **2011**, *134*, DOI 10.1063/1.3530286.

[2] S. L. Tait, Z. Dohnálek, C. T. Campbell, B. D. Kay, *J. Chem. Phys.* **2006**, *125*, DOI 10.1063/1.2400235.

[3] C. Yu, F. Wang, Y. Zhang, L. Zhao, B. Teng, M. Fan, X. Liu, *Catalysts* **2018**, *8*, 26–28.

[4] P. L. de Andres, L. de Andres-Bragado, L. Hoessly, *Front. Appl. Math. Stat.* **2021**, *7*, 1–14.

[5] F. Zaera, *Appl. Catal. A Gen.* **2002**, *229*, 75–91.

[6] S. K. Jo, *Surf. Sci.* **2015**, *635*, 99–107.

[7] D. Borodin, N. Hertl, G. B. Park, M. Schwarzer, J. Fingerhut, Y. Wang, J. Zuo, F. Nitz, G. Skoulatakis, A. Kandratsenka, D. J. Auerbach, D. Schwarzer, H. Guo, T. N. Kitsopoulos, A. M. Wodtke, **2022**, 394–398.

[8] S. Saerens, M. K. Sabbe, V. V. Galvita, E. A. Redekop, M. F. Reyniers, G. B. Marin, *ACS Catal.* **2017**, *7*, 7495–7508.

[9] Z. Lian, S. Ali, T. Liu, C. Si, B. Li, D. S. Su, *ACS Catal.* **2018**, *8*, 4694–4704.

[10] A. Baraldi, G. Comelli, S. Lizzit, D. Cocco, G. Paolucci, R. Rosei, *Surf. Sci. Lett.* **1996**, *367*.

[11] V. Johánek, V. Nehasil, T. Skála, N. Tsud, *J. Phys. Chem. C* **2019**, *123*, 7911–7921.

[12] J. S. McEwen, S. H. Payne, H. J. Kreuzer, M. Kinne, R. Denecke, H. P. Steinrück, *Surf. Sci.* **2003**, *545*, 47–69.

[13] X. Li, K. Niu, J. Zhang, X. Yu, H. Zhang, Y. Wang, Q. Guo, P. Wang, F. Li, Z. Hao, C. Xu, Y. Tang, Z. Xu, S. Lu, P. Liu, G. Xue, Y. Wei, L. Chi, *Natl. Sci. Rev.* **2021**.

[14] J. Björk, S. Stafström, F. Hanke, *J. Am. Chem. Soc.* **2011**, *133*, 14884–14887.